energies

MDPI

Article

Sliding Mode Observer with Adaptive Parameter Estimation for Sensorless Control of IPMSM

Yubo Liu, Junlong Fang *, Kezhu Tan, Boyan Huang and Wenshuai He

College of Electrical and Information, Northeast Agricultural University, Harbin 150030, China; liuyubo0821@126.com (Y.L.); kztanneau@126.com (K.T.); byhuang@neau.edu.cn (B.H.); Lisahe@neau.edu.cn (W.H.)

* Correspondence: junlongfang@126.com; Tel.: +86-1393-643-9133

Received: 30 October 2020; Accepted: 11 November 2020; Published: 17 November 2020

Abstract: To improve the observation accuracy and robustness of the sensorless control of an interior permanent magnet synchronous motor (IPMSM), a sliding mode observer based on the super twisting algorithm (STA-SMO) with adaptive parameters estimation control is proposed, as parameter mismatches are considered. First, the conventional sliding mode observer (CSMO) is analyzed. The conventional exponential approach law produces a large chattering phenomenon in the back EMF estimation, which causes a large observation error when filtering the chattering through the low-pass filter. Second, a high-order approach law of the super twisting algorithm is introduced to observe the rotor position and speed estimation, which uses the integral function to eliminate the chattering of the sliding mode. Third, an adaptive parameter estimation control (APEC) is presented to enhance the observation accuracy caused by parameter mismatches; the motor parameter adaptive law of the APEC is designed by Lyapunov's stability law. Finally, the proposed method not only reduces both the chattering and the low-pass filter, but it also enhances accuracy and robustness against parameter mismatches, as discussed through simulations and experiments.

Keywords: interior permanent magnet synchronous motor; sliding mode observer; super twisting algorithm; adaptive parameters estimation control; parameter mismatch

1. Introduction

To further improve system control performance, scholars have considered the permanent magnet synchronous motor (PMSM) to be a research subject as they are constantly exploring the advanced control theory [1]. The sensorless control of a PMSM is a kind of important approach that adapts to the bad environment and solves the problem of an inconvenient sensor installation and poor immunity [2]. The PMSM control system is demanding on the rotor position signal, which requires a good control algorithm for the stator current, and this is done by performing complex operations to find the rotor position signal.

The essence of the observer method (OBM) in feeding the construct variables back to the control system in real time and satisfying the response speed of the system is to construct nonmeasurable variables through measurable state variables. The OBM is suitable for the sensorless control of PMSMs. The OBMs include the extended Kalman filter, state observer, and sliding mode observer.

The extended Kalman filter [3–5] uses terminal signals contaminated by noise for the recursive optimal state estimation of the motor, which is computationally large, involving vector and matrix operations [6,7]. Additionally, it must be very careful in selecting the noise covariance matrix and the initial value of the algorithm to avoid instability. The state observer method combined with the concept of direct torque control of the PMSM is used to estimate the rotor position and the speed over the middle-high speed range [8]. The state observer is essentially state reconstruction, which needs to

correct the error between the observer estimate and the measured value through the feedback gain matrix in real time [9], and its feedback gain matrix parameters tuning is relatively complex.

The fundamental difference between the sliding mode observer (SMO) and the conventional observer method is the discontinuity of control, that is, the switching characteristics. The SMO ensures the convergence speed of the system and avoids the problem of the chattering through selecting the sliding mode surface and the sliding mode gain. The SMO model is insensitive to unknown nonlinear disturbances and has the advantage of strong robustness, which is superior to the extended Kalman filter in practical applications [10]. The SMO can effectively solve the complex problem of the feedback gain tuning of the state observer by the nonlinear switching term's feedback output estimation error [11]. It appropriately amplifies the output error coefficients in the feedback correction term of the SMO, which can enlarge the sliding area and accurately estimate the interference signal.

It considers the current error value obtained by comparing the observed value with the measured value to be the sliding mode surface to design the sliding mode observer (SMO) control law through the state equation of the static two-phase coordinate of the PMSM system [12–15]. By comparing the observation equation with the state equation, the estimate value of the back electromotive force (EMF) can be obtained, and the sliding mode gain can be designed by Lyapunov's stability condition. However, the conventional sliding mode observer (CSMO) is required to be filtered, thus affecting the observation accuracy of the system, which has switching chattering during the observation of the back EMF. In [16,17], a sliding mode observer control law that was designed by fractional order theory effectively weakened the chattering of the system. In [18–20], an adaptive exponential approach law was proposed by combining the first-order norm and the switching function law into the conventional approach law. According to the change of the sliding mode surface and system state, the convergence speed of the system can be adjusted adaptively, and the high frequency chattering of the back EMF can be reduced. However, this adaptive exponential approach law always has complex parameter tuning. In [21], an improved sliding mode observer that uses a hyperbolic tangent function instead of sign function effectively eliminates the chattering during high speed operation and realizes the accurate estimation of the rotor position and speed. Changing the switch function and treating the boundary layer continuously does not completely solve the effect of switch chattering. Therefore, a high-order sliding mode control law [22–24] was designed to eliminate the chattering. The control signal of the observer is smooth enough to be used directly to estimate the back EMF, and thus the phase lag of the back EMF caused by a low-pass filter is avoided. In [25], the super twisting second-order sliding mode algorithm was improved, the convergence of the observer was proven, and the range of the observer gain was given.

However, these methods have an inadaptive ability. The change of the motor parameters affects the observation results, bring deviation to the estimation of the rotor position and speed. Improving the observation accuracy of the SMO and reducing the parameter dependence of the algorithm becomes the key technical problem for sensorless control of PMSMs.

Due to the problem of the motor parameter mismatches influencing the estimation of the back EMF, an adaptive sliding mode observer method was proposed [26]. This method, which constructs Lyapunov's stability law, while deducing the adaptive law of resistance parameters and effectively tracking the change of resistance parameters, effectively suppresses the influence of the motor resistance parameter mismatches on the observation results. A current sliding mode observer method for the resistance estimation that effectively tracks the actual value of the resistance and reduces the influence of the resistance change on the back EMF observation was proposed [27]. The observer in the rotating coordinate system was constructed for the estimation of the motor resistance, and the switch chattering was filtered by a low-pass filter. In [28,29], an approach was proposed to combine the model reference adaptive method with the second-order sliding mode to realize the accurate estimation of the back EMF. The adaptive law of the stator resistance and the speed is derived from the Lyapunov stability equation. The speed estimation can be adjusted adaptively, in turn weakening the sliding mode chattering effectively. The above methods, which effectively improve the robustness of the motor parameter

mismatch system, have no mention of an effective scheme for the inductance parameter change on the estimation of the back EMF. Meanwhile, the methods proposed do not take into account the characteristics of the dq-axis inductance inequality of the interior permanent magnet synchronous motor (IPMSM), which are limited to the surface mounted permanent magnet synchronous motor (SPMSM).

In this paper, an adaptive parameter estimation controller (APEC) in conjunction with a sliding mode observer based on the super twisting algorithm (STA-SMO) is proposed to realize the sensorless control of the IPMSM system. The STA-SMO is proposed to avoid the introduction of the low-pass filter, thereby reducing the chattering of the sliding mode and improving the observation accuracy of the observer. The motor parameter adaptive law of the APEC for the estimation of the rotor position and speed is analyzed by Lyapunov's stability law. The APEC combines the theory of Lyapunov's stability law and the merit of the adaptive parameter estimation in the speed loop, which forces the rotor position and speed estimation to be unaffected by the motor parameter mismatches and has strong robustness.

The basic theoretical background of the CSMO is presented in Section 2. The STA-SMO model design and its stability analysis are presented in Section 3. The STA-SMO model design with parameter mismatches and the APEC law design are presented in Section 4. Sections 5 and 6 provide the results by simulation and experiment. Finally, results discussion and conclusions are summarized in Sections 7 and 8.

2. Sensorless Control Model Based on Conventional Sliding Mode Observer

2.1. State Space Equation of the IPMSM

The electromagnetism equation and the motion equation for the three-phase IPMSM have already been given in detail and are therefore not detailed in this paper. The αβ-axis stator voltage equation for the IPMSM is characterized by the following equations:

$$\frac{d}{dt}\begin{bmatrix} i_\alpha \\ i_\beta \end{bmatrix} = \hat{A}\begin{bmatrix} i_\alpha \\ i_\beta \end{bmatrix} + \frac{1}{L_d}\begin{bmatrix} u_\alpha \\ u_\beta \end{bmatrix} - \frac{1}{L_d}\begin{bmatrix} E_\alpha \\ E_\beta \end{bmatrix} \tag{1}$$

where $\hat{A} = \begin{bmatrix} -\frac{\hat{R}_s}{\hat{L}_d} & -\frac{(\hat{L}_d-\hat{L}_q)\omega_e}{\hat{L}_d} \\ \frac{(\hat{L}_d-\hat{L}_q)\omega_e}{\hat{L}_d} & -\frac{\hat{R}_s}{\hat{L}_d} \end{bmatrix}$; u_α and u_β are the αβ-axis components of the stator voltages, respectively; i_α and i_β are the αβ-axis components of the stator currents, respectively; E_α and E_β are the αβ-axis components of the back EMF, respectively; $\hat{L}_d$ and $\hat{L}_q$ are the dq-axis components of the inductances estimated values, respectively; $\hat{R}_s$ is the estimated value of the motor resistance; and ω_e is the rotor electric speed.

The back EMF equation can be expressed as

$$\begin{bmatrix} E_\alpha \\ E_\beta \end{bmatrix} = \left[(\hat{L}_d - \hat{L}_q)(\omega_e i_d - \frac{di_q}{dt}) + \omega_e \varphi_f\right]\begin{bmatrix} -sin\theta \\ cos\theta \end{bmatrix} \tag{2}$$

where θ is the rotor position.

2.2. Models of the Conventional Sliding Mode Observer

To obtain the estimated value of the back EMF, the CSMO is designed as

$$\frac{d}{dt}\begin{bmatrix} \hat{i}_\alpha \\ \hat{i}_\beta \end{bmatrix} = \hat{A}\begin{bmatrix} \hat{i}_\alpha \\ \hat{i}_\beta \end{bmatrix} + \frac{1}{\hat{L}_d}\begin{bmatrix} u_\alpha \\ u_\beta \end{bmatrix} - \begin{bmatrix} u_{smo\alpha} \\ u_{smo\beta} \end{bmatrix} \tag{3}$$

where $\hat{i}_\alpha$ and $\hat{i}_\beta$ are the αβ-axis components of the current estimated values, respectively; $u_{smo\alpha}$ and $u_{smo\beta}$ are the αβ-axis components of the control laws for the CSMO.

Comparing Equation (3) with Equation (1), the error equation of the stator current can be obtained as

$$\frac{d}{dt}\begin{bmatrix} \widetilde{i}_\alpha \\ \widetilde{i}_\beta \end{bmatrix} = \hat{A}\begin{bmatrix} \widetilde{i}_\alpha \\ \widetilde{i}_\beta \end{bmatrix} + \frac{1}{\hat{L}_d}\begin{bmatrix} E_\alpha \\ E_\beta \end{bmatrix} - \begin{bmatrix} u_{smo\alpha} \\ u_{smo\beta} \end{bmatrix} \tag{4}$$

where $\widetilde{i}_\alpha = \hat{i}_\alpha - i_\alpha$ and $\widetilde{i}_\beta = \hat{i}_\beta - i_\beta$ are the errors of the current observations.

The errors of the current observations are designed as sliding surfaces:

$$s = \begin{bmatrix} s_\alpha \\ s_\beta \end{bmatrix} = \begin{bmatrix} \widetilde{i}_\alpha \\ \widetilde{i}_\beta \end{bmatrix} \tag{5}$$

When the system is in the sliding mode area, $\dot{s} = 0$. Then,

$$\dot{s} = \begin{bmatrix} \dot{s}_\alpha \\ \dot{s}_\beta \end{bmatrix} = A\begin{bmatrix} \widetilde{i}_\alpha \\ \widetilde{i}_\beta \end{bmatrix} - \begin{bmatrix} u_{smo\alpha} \\ u_{smo\beta} \end{bmatrix} = 0 \tag{6}$$

2.3. Sliding Mode Control Function

The CSMO adopts the constant approach law, and the control law is given as

$$\begin{bmatrix} u_{smo\alpha} \\ u_{smo\beta} \end{bmatrix} = \hat{A}\begin{bmatrix} \widetilde{i}_\alpha \\ \widetilde{i}_\beta \end{bmatrix} + \begin{bmatrix} K_\alpha sgn\left(\widetilde{i}_\alpha\right) \\ K_\beta sgn\left(\widetilde{i}_\beta\right) \end{bmatrix} \tag{7}$$

where K_α and K_β are the switching gains of the constancy approach law; $sgn(x)$ is the symbolic function: $x \geq 0$, $sgn(x) = 1$; $x < 0$, $sgn(x) = -1$.

When the observer state variable reaches the sliding mode surface, the system is stable, and the current error is zero. From Equations (4) and (7), it can be obtained as

$$\begin{bmatrix} E_\alpha \\ E_\beta \end{bmatrix} = \begin{bmatrix} \hat{L}_d K_\alpha sgn\left(\widetilde{i}_\alpha\right) \\ \hat{L}_d K_\beta sgn\left(\widetilde{i}_\beta\right) \end{bmatrix} \tag{8}$$

The CSMO that produces a high frequency buffeting signal because its switching function often combines the filter to obtain the smooth back EMF observations. However, a phase lag problem is introduced by the filter, in turn reducing observation accuracy.

2.4. Stability Analysis of the CSMO

The stability conditions of the CSMO are obtained, with the Lyapunov function $\dot{V}(x) = s\dot{s} \leq 0$. It follows from Equations (5)–(7) and the reachability condition that

$$\dot{V}(x) = \begin{bmatrix} s_\alpha \dot{s}_\alpha \\ s_\beta \dot{s}_\beta \end{bmatrix} = \begin{bmatrix} s_\alpha (\frac{E_\alpha}{\hat{L}_d} - K_\alpha sgn(\widetilde{i}_\alpha)) \\ s_\beta (\frac{E_\beta}{\hat{L}_d} - K_\beta sgn(\widetilde{i}_\beta)) \end{bmatrix} \leq 0 \tag{9}$$

Guaranteeing $\dot{V}(x) \leq 0$, it can be sure that the asymptotic stability of the control system is obtained. Thus, the switching gains must satisfy Equation (10).

$$\begin{cases} K_\alpha \geq \frac{1}{\hat{L}_d}|E_\alpha| \\ K_\beta \geq \frac{1}{\hat{L}_d}\left|E_\beta\right| \end{cases} \tag{10}$$

2.5. Rotor Position and Speed Estimation Based on Phase Locked Loop

The rotor position estimation method based on the tangent function amplifies the switching chattering of the back EMF, thus causing the angle estimation error. When $\left|\theta_e - \hat{\theta}_e\right| < \pi/6, sin(\theta_e - \hat{\theta}_e) = \theta_e - \hat{\theta}_e$, it can be obtained as

$$\begin{aligned} \Delta E &= -\hat{E}_\alpha cos\hat{\theta}_e - \hat{E}_\beta sin\hat{\theta}_e \\ &= ksin\theta_e cos\hat{\theta}_e - kcos\theta_e sin\hat{\theta}_e \\ &= ksin(\theta_e - \hat{\theta}_e) \approx k(\theta_e - \hat{\theta}_e) \end{aligned} \tag{11}$$

where $k = (\hat{L}_d - \hat{L}_q)(\omega_e i_d - \frac{di_q}{dt}) + \omega_e \psi_f$.

Equation (11) shows that the rotor position error value is obtained by comparing the actual rotor position with the estimated position of the motor. It is adjusted by the PI regulator to generate the rotor speed estimated value. The rotor position can be estimated by the integral operation on the estimated value of the rotor speed. A block diagram of the phase locked loop (PLL) is shown in Figure 1. The structure diagram of the CSMO for sensorless control of IPMSM is shown in Figure 2.

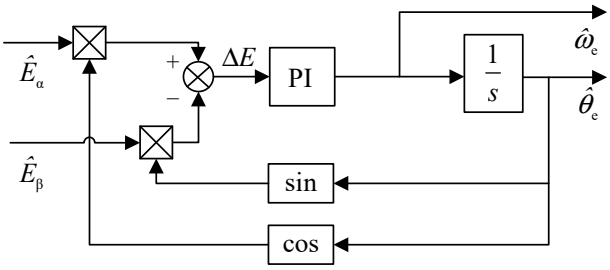

Figure 1. Block diagram of PLL.

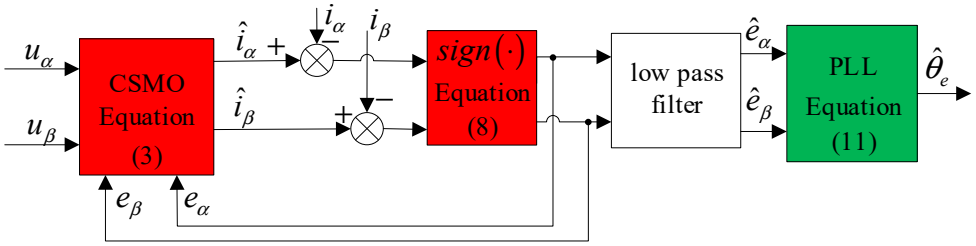

Figure 2. Conventional sliding mode observer structure diagram.

3. Sliding Mode Observer Based on Super Twisting Algorithm

3.1. Models of the STA-SMO

A method of the sliding mode approach law is proposed, based on the super twisting algorithm (STA), which eliminates the inherent chattering of a sliding mode control through using an integral to deal with the switch function, while saving the filter link, and improves the observation accuracy.

The sliding mode observer model based on STA is designed as

$$\frac{d}{dt}\begin{bmatrix} \hat{i}_\alpha \\ \hat{i}_\beta \end{bmatrix} = \hat{A}\begin{bmatrix} \hat{i}_\alpha \\ \hat{i}_\beta \end{bmatrix} + \frac{1}{\hat{L}_d}\begin{bmatrix} u_\alpha \\ u_\beta \end{bmatrix} - \begin{bmatrix} u_{sta\alpha} \\ u_{sta\beta} \end{bmatrix} \tag{12}$$

where $u_{sta\alpha}$ and $u_{sta\beta}$ are the control laws for the STA-SMO, respectively.

Comparing Equation (12) with Equation (1), the error equation of the stator current can be obtained as

$$\frac{d}{dt}\begin{bmatrix} \tilde{i}_\alpha \\ \tilde{i}_\beta \end{bmatrix} = \hat{A}\begin{bmatrix} \tilde{i}_\alpha \\ \tilde{i}_\beta \end{bmatrix} + \frac{1}{\hat{L}_d}\begin{bmatrix} E_\alpha \\ E_\beta \end{bmatrix} - \begin{bmatrix} u_{sta\alpha} \\ u_{sta\beta} \end{bmatrix} \tag{13}$$

where $\tilde{i}_\alpha = \hat{i}_\alpha - i_\alpha$ and $\tilde{i}_\beta = \hat{i}_\beta - i_\beta$ are the errors of the current observations.

The errors of the current observations are designed as sliding surfaces:

$$s = \begin{bmatrix} s_\alpha \\ s_\beta \end{bmatrix} = \begin{bmatrix} \widetilde{i}_\alpha \\ \widetilde{i}_\beta \end{bmatrix} \tag{14}$$

When the system is in the sliding mode area, $\dot{s} = 0$. Then,

$$\dot{s} = \begin{bmatrix} \dot{s}_\alpha \\ \dot{s}_\beta \end{bmatrix} = A\begin{bmatrix} \widetilde{i}_\alpha \\ \widetilde{i}_\beta \end{bmatrix} - \begin{bmatrix} u_{\mathrm{smo}\alpha} \\ u_{\mathrm{smo}\beta} \end{bmatrix} = 0 \tag{15}$$

3.2. Sliding Mode Control Function

The STA-SMO adopts the STA approach law, and the control law is given as

$$\dot{s} = \begin{bmatrix} -k_1\left|\widetilde{i}_\alpha\right|^{1/2} sign(\widetilde{i}_\alpha) - k_2\int sgn(\widetilde{i}_\alpha)dt \\ -k_1\left|\widetilde{i}_\beta\right|^{1/2} sign(\widetilde{i}_\beta) - k_2\int sgn(\widetilde{i}_\beta)dt \end{bmatrix} \tag{16}$$

where k_1 and k_2 are the switching gains of the improved STA approach law, and $sgn(x)$ is the symbolic function: $x \geq 0$, $sgn(x) = 1$; $x < 0$, $sgn(x) = -1$.

When the system is in the sliding mode area, $\dot{s} = 0$. Then, the STA-SMO control law is given as

$$\begin{bmatrix} u_{\mathrm{sta}\alpha} \\ u_{\mathrm{sta}\beta} \end{bmatrix} = \hat{A}\begin{bmatrix} \widetilde{i}_\alpha \\ \widetilde{i}_\beta \end{bmatrix} + \begin{bmatrix} k_1\left|\widetilde{i}_\alpha\right|^{1/2} sgn(\widetilde{i}_\alpha) + k_2\int sgn(\widetilde{i}_\alpha)dt \\ k_1\left|\widetilde{i}_\beta\right|^{1/2} sgn(\widetilde{i}_\beta) + k_2\int sgn(\widetilde{i}_\beta)dt \end{bmatrix} \tag{17}$$

When the observer state variable reaches the sliding mode surface, the system is stable and the current error is zero. From Equation (13), it can be obtained as

$$\begin{bmatrix} E_\alpha \\ E_\beta \end{bmatrix} = \hat{L}_\mathrm{d}\begin{bmatrix} k_1\left|\widetilde{i}_\alpha\right|^{1/2} sgn(\widetilde{i}_\alpha) + k_2\int sgn(\widetilde{i}_\alpha)dt \\ k_1\left|\widetilde{i}_\beta\right|^{1/2} sgn(\widetilde{i}_\beta) + k_2\int sgn(\widetilde{i}_\beta)dt \end{bmatrix} \tag{18}$$

As seen from the observations of the back EMF, the STA sliding mode control law uses an integral filter to deal with the switch function effectively in order to suppress chattering phenomenon while reducing low-pass filtering to avoid phase delay.

3.3. Stability Analysis of the STA-SMO

In [30,31], the stability of the super twisting algorithm has been proven, and the tuning range of the parameters is given as

$$\hat{A}\begin{bmatrix} \hat{i}_\alpha \\ \hat{i}_\beta \end{bmatrix} + \frac{1}{\hat{L}_\mathrm{d}}\begin{bmatrix} u_\alpha \\ u_\beta \end{bmatrix} \leq \delta\begin{bmatrix} \left|\widetilde{i}_\alpha\right|^{1/2} \\ \left|\widetilde{i}_\beta\right|^{1/2} \end{bmatrix} \tag{19}$$

where δ, k_1, and k_2 must satisfy Equation (19).

$$k_1 > 2\delta, k_2 > k_1\frac{5\delta k_1 + 4\delta^2}{2(k_1 - 2\delta)} \tag{20}$$

A structure diagram of the sliding mode observer based on the super twisting algorithm is shown in Figure 3. The current error value, which is obtained by comparing the current value estimated by the SMO with the actual current value, is the foundation of the sliding mode surface. Then, the sliding mode approach law based on the super twisting algorithm is designed to estimate the back EMF signal.

The estimated back EMF is used as the input of the PLL to estimate the rotor position and speed of the IPMSM.

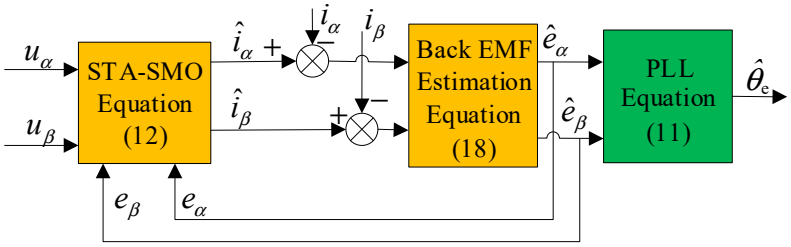

Figure 3. Sliding mode observer based on the super twisting structure diagram.

4. Adaptive Parameters Estimation Control

4.1. Impact Analysis of Parameters Mismatch of the IPMSM

A STA-SMO that considers motor parameter mismatches is designed as

$$\frac{d}{dt}\begin{bmatrix} \hat{i}_\alpha \\ \hat{i}_\beta \end{bmatrix} = A\begin{bmatrix} \hat{i}_\alpha \\ \hat{i}_\beta \end{bmatrix} + \frac{1}{L_d}\begin{bmatrix} u_\alpha \\ u_\beta \end{bmatrix} - \begin{bmatrix} u_{smo\alpha} \\ u_{smo\beta} \end{bmatrix} \tag{21}$$

where $A = \begin{bmatrix} -\frac{R_s}{L_d} & -\frac{(L_d - L_q)\omega_e}{L_d} \\ \frac{(L_d - L_q)\omega_e}{L_d} & -\frac{R_s}{L_d} \end{bmatrix}$; the actual value of resistance is $R_s = \hat{R}_s + \Delta R_s$; $L_d = \hat{L}_d + \Delta L_d$ and $L_q = \hat{L}_q + \Delta L_q$ are the actual value of motor inductances; ΔR_s, ΔL_d, and ΔL_q are the deviation between the actual values and the estimated values.

Separating the deviation of Equation (21), the equivalent equation can be obtained as

$$\frac{d}{dt}\begin{bmatrix} \hat{i}_\alpha \\ \hat{i}_\beta \end{bmatrix} = \hat{A}\begin{bmatrix} \hat{i}_\alpha \\ \hat{i}_\beta \end{bmatrix} + \frac{1}{\hat{L}_d}\begin{bmatrix} u_\alpha \\ u_\beta \end{bmatrix} - \begin{bmatrix} u_{smo\alpha} \\ u_{smo\beta} \end{bmatrix} + \Delta A\begin{bmatrix} \hat{i}_\alpha \\ \hat{i}_\beta \end{bmatrix} - \frac{\Delta L_d}{\hat{L}_d}\frac{d}{dt}\begin{bmatrix} \hat{i}_\alpha \\ \hat{i}_\beta \end{bmatrix} \tag{22}$$

where $\Delta A = \begin{bmatrix} -\frac{\Delta R_s}{\hat{L}_d} & -\frac{(\Delta L_d - \Delta L_q)\omega_e}{\hat{L}_d} \\ \frac{(\Delta L_d - \Delta L_q)\omega_e}{\hat{L}_d} & -\frac{\Delta R_s}{\hat{L}_d} \end{bmatrix}$.

Comparing Equation (22) with Equation (3), the error equation of the stator current can be obtained as

$$\frac{d}{dt}\begin{bmatrix} \widetilde{i}_\alpha \\ \widetilde{i}_\beta \end{bmatrix} = \hat{A}\begin{bmatrix} \widetilde{i}_\alpha \\ \widetilde{i}_\beta \end{bmatrix} + \frac{1}{\hat{L}_d}\begin{bmatrix} E_{t\alpha} \\ E_{t\beta} \end{bmatrix} - \begin{bmatrix} u_{sta\alpha} \\ u_{sta\beta} \end{bmatrix} + \Delta A\begin{bmatrix} \hat{i}_\alpha \\ \hat{i}_\beta \end{bmatrix} - \frac{\Delta L_d}{\hat{L}_d}\frac{d}{dt}\begin{bmatrix} \hat{i}_\alpha \\ \hat{i}_\beta \end{bmatrix} \tag{23}$$

The STA-SMO based on the deviation of the motor parameters can still satisfy the convergence of the stator current in the effective time, whose sliding mode gain satisfies Equation (23) under parameter mismatch.

$$\begin{bmatrix} E_{t\alpha} \\ E_{t\beta} \end{bmatrix} = \hat{L}_d\begin{bmatrix} k_1\left|\widetilde{i}_\alpha\right|^{1/2} sgn(\widetilde{i}_\alpha) + k_2\int sgn(\widetilde{i}_\alpha)dt \\ k_1\left|\widetilde{i}_\beta\right|^{1/2} sgn(\widetilde{i}_\beta) + k_2\int sgn(\widetilde{i}_\beta)dt \end{bmatrix} - \hat{L}_d\Delta A\begin{bmatrix} \hat{i}_\alpha \\ \hat{i}_\beta \end{bmatrix} + \Delta L_d\frac{d}{dt}\begin{bmatrix} \hat{i}_\alpha \\ \hat{i}_\beta \end{bmatrix} \tag{24}$$

Comparing Equation (24) with Equation (18), the back EMF after parameter change is given as

$$\begin{bmatrix} E_{t\alpha} \\ E_{t\beta} \end{bmatrix} = \begin{bmatrix} E_\alpha \\ E_\beta \end{bmatrix} - \hat{L}_d\Delta A\begin{bmatrix} \hat{i}_\alpha \\ \hat{i}_\beta \end{bmatrix} + \Delta L_d\frac{d}{dt}\begin{bmatrix} \hat{i}_\alpha \\ \hat{i}_\beta \end{bmatrix} \tag{25}$$

where E_α and E_β are the estimated back EMF; $E_{t\alpha}$ and $E_{t\beta}$ are the real values of the back EMF with the change of the motor parameters.

As seen from Equation (25), the deviation of motor parameters, the current, the current change rate, and the speed affect the amplitude and phase of the back EMF estimation. In [23], a vector diagram is drawn to explain the influence of motor parameter mismatches on the back EMF estimation of the SPMSM in detail. The $i_d = 0$ control mode of the SPMSM is that the back EMF is perpendicular to the rotor flux (the stator current vector is parallel to the q axis), which is in the same phase as the stator current vector. As seen from Equation (2), the d-axis component exists in the control mode, which causes the back EMF direction of the IPMSM to be different from the stator current vector. Compared with the SPMSM, the parameter mismatch, the current, the current change rate, and the speed of the IPMSM have complex effects on the amplitude and the phase of the back EMF estimation. However, the parameter mismatches, the current, the current change rate, and the speed change; the phase of the back EMF estimation is deviated, which affects the system's estimation of the rotor position and speed.

4.2. STA-SMO with Adaptive Parameters Estimation Control

The STA-SMO with adaptive parameter estimation control is based on the Lyapunov stability condition ($v\dot{v} \le 0$). From Equation (22), the Lyapunov function can be determined as

$$v = \frac{1}{2}s^T s^2 + \frac{1}{2}\Delta R_s{}^2 + \frac{1}{2}\Delta L_d{}^2 + \frac{1}{2}\Delta L_q{}^2 \tag{26}$$

where $s = \begin{bmatrix} \widetilde{i}_\alpha \\ \widetilde{i}_\beta \end{bmatrix}$.

Substituting Equation (22) into Equation (26) with Lyapunov stability conditions, it is provides that

$$\begin{bmatrix} s_\alpha & s_\beta \end{bmatrix} \begin{bmatrix} \frac{E_\alpha}{L_d} - k_1\left|\widetilde{i}_\alpha\right|^{1/2} sgn(\widetilde{i}_\alpha) - k_2\int sgn(\widetilde{i}_\alpha)dt - \frac{\Delta R_s}{L_d}\hat{i}_\alpha - \frac{(\Delta L_d - \Delta L_q)\omega_e}{L_d}\hat{i}_\beta - \frac{\Delta L_d}{L_d}\frac{d\hat{i}_\alpha}{dt} \\ \frac{E_\beta}{L_d} - k_1\left|\widetilde{i}_\beta\right|^{1/2} sgn(\widetilde{i}_\beta) - k_2\int sgn(\widetilde{i}_\beta)dt + \frac{(\Delta L_d - \Delta L_q)\omega_e}{L_d}\hat{i}_\alpha - \frac{\Delta R_s}{L_d}\hat{i}_\beta - \frac{\Delta L_d}{L_d}\frac{d\hat{i}_\beta}{dt} \end{bmatrix} + \Delta R_s\Delta\dot{R}_s + \Delta L_d\Delta\dot{L}_d + \Delta L_q\Delta\dot{L}_q \le 0 \tag{27}$$

It follows from Equation (21) and the stability condition that

$$\begin{bmatrix} s_\alpha & s_\beta \end{bmatrix} \begin{bmatrix} \frac{E_\alpha}{L_d} - k_1\left|\widetilde{i}_\alpha\right|^{1/2} sgn(\widetilde{i}_\alpha) - k_2\int sgn(\widetilde{i}_\alpha)dt \\ \frac{E_\beta}{L_d} - k_1\left|\widetilde{i}_\beta\right|^{1/2} sgn(\widetilde{i}_\beta) - k_2\int sgn(\widetilde{i}_\beta)dt \end{bmatrix} \le 0 \tag{28}$$

$$\begin{bmatrix} s_\alpha & s_\beta \end{bmatrix} \begin{bmatrix} -\frac{\Delta R_s}{L_d}\hat{i}_\alpha \\ -\frac{\Delta R_s}{L_d}\hat{i}_\beta \end{bmatrix} + \Delta R_s\Delta\dot{R}_s = 0 \tag{29}$$

$$\begin{bmatrix} s_\alpha & s_\beta \end{bmatrix} \begin{bmatrix} -\frac{\Delta L_d\omega_e}{L_d}\hat{i}_\beta - \frac{\Delta L_d}{L_d}\frac{d\hat{i}_\alpha}{dt} \\ \frac{\Delta L_d\omega_e}{L_d}\hat{i}_\alpha - \frac{\Delta L_d}{L_d}\frac{d\hat{i}_\beta}{dt} \end{bmatrix} + \Delta L_d\Delta\dot{L}_d = 0 \tag{30}$$

$$\begin{bmatrix} s_\alpha & s_\beta \end{bmatrix} \begin{bmatrix} \frac{\Delta L_q\omega_e}{L_d}\hat{i}_\beta \\ -\frac{\Delta L_q\omega_e}{L_d}\hat{i}_\alpha \end{bmatrix} + \Delta L_q\Delta\dot{L}_q = 0 \tag{31}$$

From Equations (29)–(31), the derivative equation of the motor parameter deviation is derived as

$$\begin{cases} \Delta\dot{R}_s = \frac{1}{L_d}s_\alpha\hat{i}_\alpha + \frac{1}{L_d}s_\beta\hat{i}_\beta \\ \Delta\dot{L}_d = \frac{\omega_e}{L_d}s_\alpha\hat{i}_\beta - \frac{\omega_e}{L_d}s_\beta\hat{i}_\alpha + \frac{1}{L_d}s_\alpha\frac{d\hat{i}_\alpha}{dt} + \frac{1}{L_d}s_\beta\frac{d\hat{i}_\beta}{dt} \\ \Delta\dot{L}_q = -\frac{\omega_e}{L_d}s_\alpha\hat{i}_\beta + \frac{\omega_e}{L_d}s_\beta\hat{i}_\alpha \end{cases} \tag{32}$$

From the definition of motor parameter deviation, $\dot{R}_s = \Delta\dot{R}_s$, $\dot{L}_d = \Delta\dot{L}_d$, and $\dot{L}_q = \Delta\dot{L}_q$, the motor parameter estimation equation can be obtained as

$$\begin{cases} \dot{R}_s = \frac{1}{L_d} s_\alpha \hat{i}_\alpha + \frac{1}{L_d} s_\beta \hat{i}_\beta \\ \dot{L}_d = \frac{\omega_e}{L_d} s_\alpha \hat{i}_\beta - \frac{\omega_e}{L_d} s_\beta \hat{i}_\alpha + \frac{1}{L_d} s_\alpha \frac{d\hat{i}_\alpha}{dt} + \frac{1}{L_d} s_\beta \frac{d\hat{i}_\beta}{dt} \\ \dot{L}_q = -\frac{\omega_e}{L_d} s_\alpha \hat{i}_\beta + \frac{\omega_e}{L_d} s_\beta \hat{i}_\alpha \end{cases} \tag{33}$$

The estimation of the motor parameters is satisfied in Equation (33), which should ensure the asymptotic stability of the system.

A block diagram of the STA-SMO with APEC is shown in Figure 4. A block diagram of the sensorless control of the IPMSM system is shown in Figure 5.

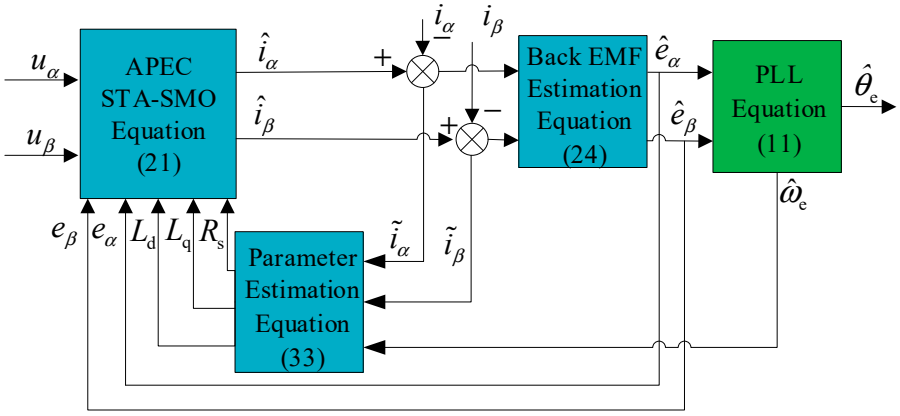

Figure 4. Structure diagram of the sliding mode observer based on the super twisting algorithm (STA-SMO) with adaptive parameter estimation control (APEC).

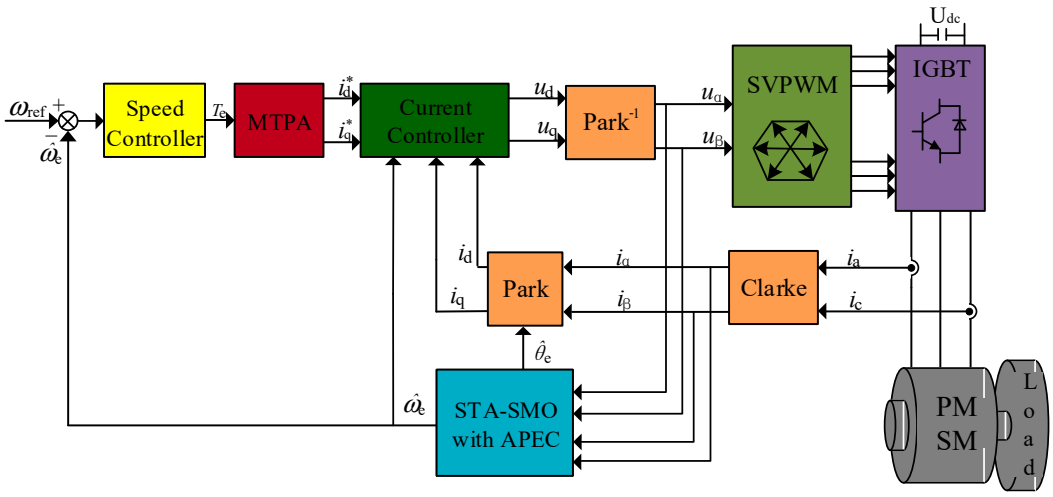

Figure 5. Control system structure diagram.

5. System Simulation Experiment

To verify the effectiveness of the designed controller, a control system model was established by MATLAB/SIMULINK. The parameters of the experimental IPMSM in the subject are shown in Table 1. The parameters of the controllers whose maximum were calculated from Equation (10) (Equation (19)) and reduced by debugging through the convergence speed, and the sliding mode chattering are shown in Table 2.

Table 1. PMSM parameters.

Parameter	Value
Rated power/(kW)	5
Rated speed/(r/min)	2500
Moment of inertia/(kg·m^2)	0.06
Friction coefficient/(N·m·s)	0.008
Polar logarithm	4
Permanent magnet flux linkage/(Wb)	0.071
Stator inductance L_d/(mH)	0.22
Stator inductance L_q/(mH)	0.61
Stator resistance/(Ω)	0.03

Table 2. Controller parameters.

Parameter	Value
K_p	30
K_i	450
k_1	13
k_2	270

Setting the motor speed to 1250 r/min, the load torque was 9 N · m in 0–1.2 s. Figures 6 and 7 show the simulation comparison of the CSMO and the STA-SMO. The blue curves represent the actual motor speed values in Figures 6a and 7a. As shown, compared with the STA-SMO, the CSMO has the greatest fluctuation to the speed estimation.

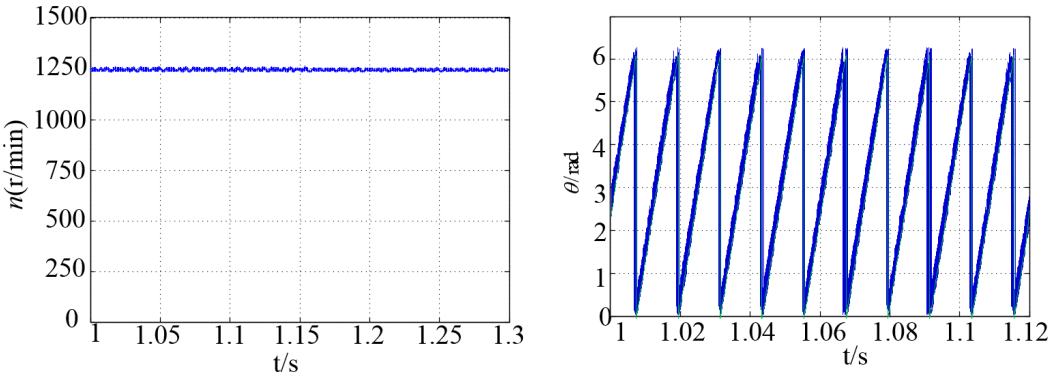

(**a**) Speed curve (**b**) Position angle curve

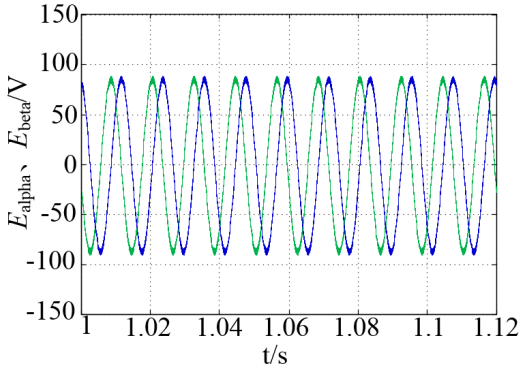

(**c**) Back EMF curve

Figure 6. Simulation curves of steady state of the conventional sliding mode observer (CSMO).

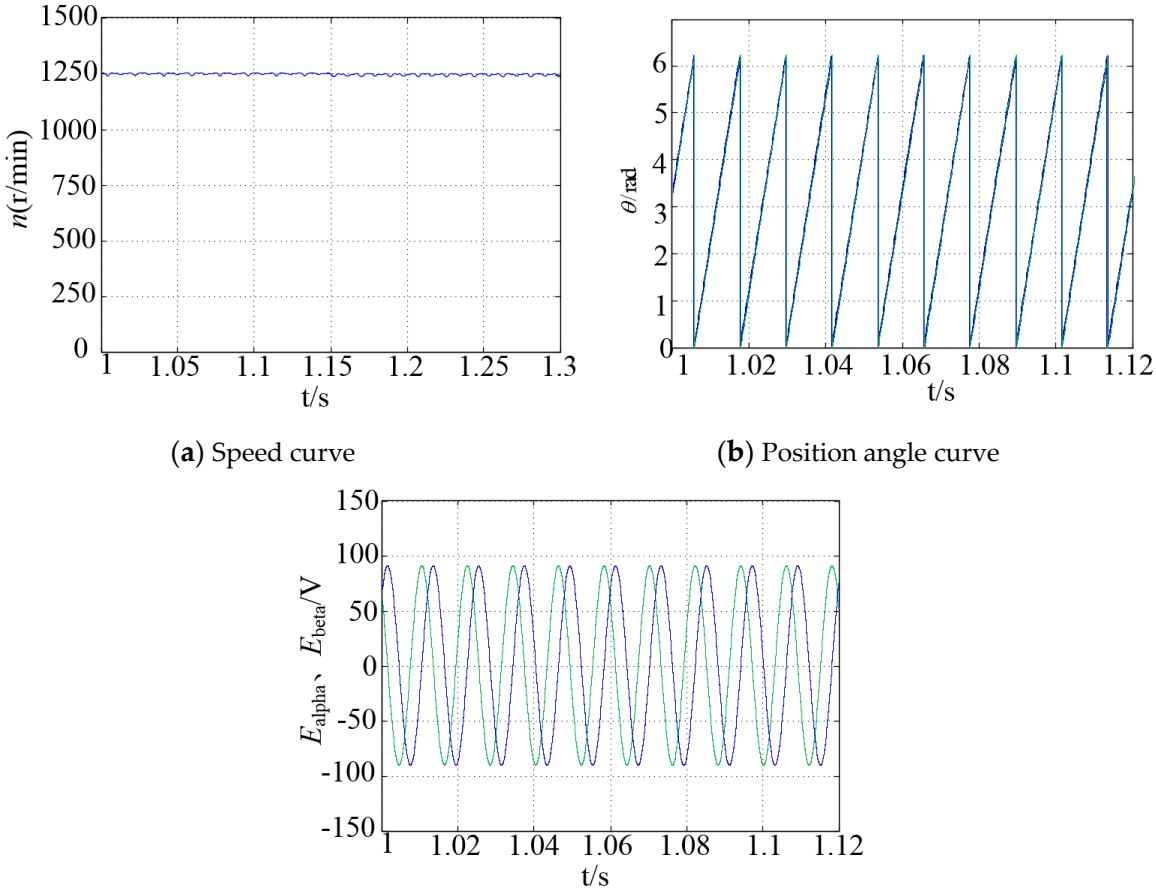

(**a**) Speed curve

(**b**) Position angle curve

(**c**) Back EMF curve

Figure 7. Simulation curves of steady state of an STA-SMO.

The blue curves represent the motor position angle estimate, and the green curves represent the actual value of the motor position angle in Figures 6b and 7b. As shown, the CSMO has a strong chattering phenomenon for the rotor position estimation, and it is a large deviation between the position angle estimation value and the actual value, which affects the system performance. With the STA-SMO, the rotor position and speed estimates are smoother, tracking the actual values is better, and the feedback system is more stable. The blue and green curves of Figures 6c and 7c are the estimated values of the back EMF in the static two-phase coordinate system, respectively. In Figure 6c, there are a large number of harmonics caused by switching chattering in the back EMF waveform, while in Figure 7c, the sinusoidal degree of the back EMF is better.

When the load torque was set to 9 N · m, the motor speed went to 1250 r/min in 0–0.6 s and increased to 2500 r/min when $t = 0.6$ s. Changing the resistance parameters ($R_s = 1.2\hat{R}_s$) and inductance parameters ($L_d = 1.2\hat{L}_d$, $L_q = 0.8\hat{L}_q$) of the motor parameters forces the motor parameters to be mismatched with the observer parameters. Figures 8 and 9 show the simulation comparison of the STA-SMO with APEC and the STA-SMO.

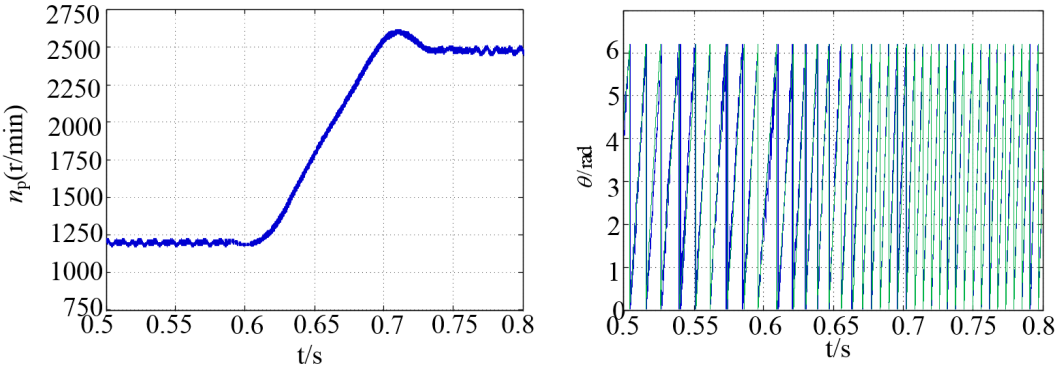

(**a**) Speed curve (**b**) Position angle curve

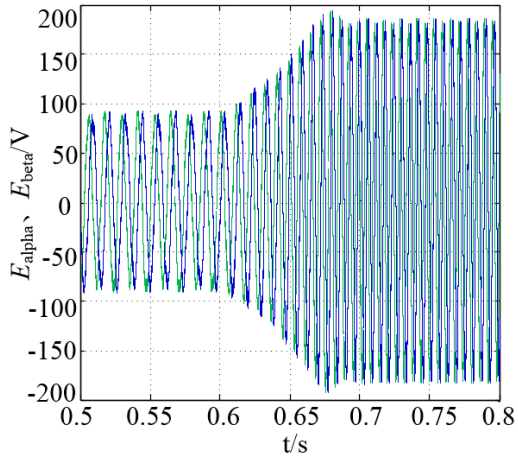

(**c**) Back EMF curve

Figure 8. Simulation response curves of the STA-SMO.

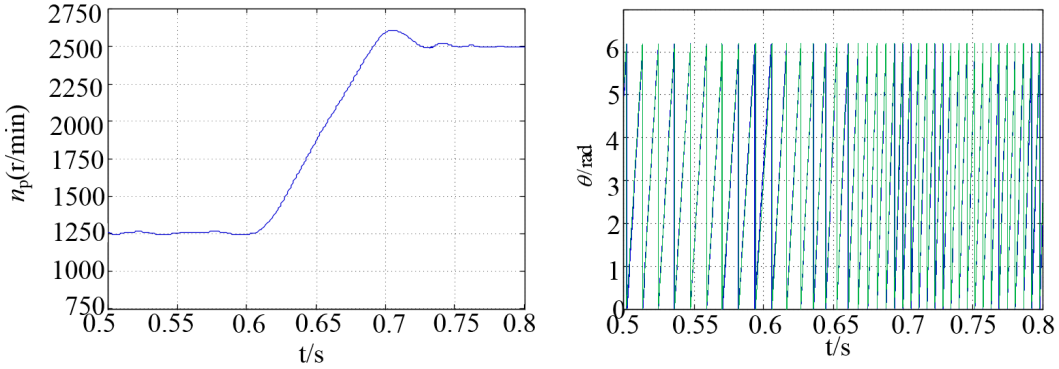

(**a**) Speed curve (**b**) Position angle curve

Figure 9. *Cont.*

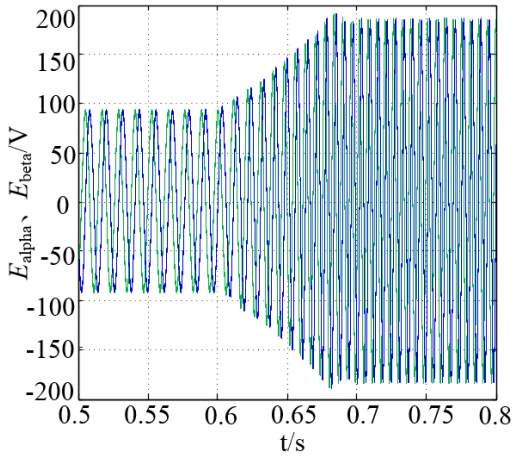

(**c**) Back EMF curve

Figure 9. Simulation response curves of the STA-SMO with APEC.

The STA-SMO parameters are mismatched when the motor parameters change: The speed estimation waveform produces larger chattering, the dynamic adjustment time is longer, and the approach process of position angle estimation waveform before reaching the sliding mode surface has produced strong chattering. It can be determined that the method uses large switching chattering in exchange for system robustness. The STA-SMO with APEC adjusts the observer parameters in real time by estimating the motor parameters and effectively tracks the actual values of position and speed. The position error is obviously smaller than that of the STA-SMO. When the motor parameters change, the system can smoothly transition this process so that the observer parameters are updated.

The STA-SMO parameters are mismatched with the motor parameters; the estimated back EMF produces fluctuations in the amplitude and phase, containing a large number of harmonics generated by the switching chattering. The sinusoidal degree of the back EMF is better and the accuracy is higher, when it adopts the STA-SMO with APEC.

6. Experimental Verification

The experimental platform includes a IPMSM, a motor controller, a dynamometer, and the measuring equipment, and a host computer is mainly responsible for the completion of the IPMSM drive control experiment and the collection of the information in the experiment process. The experimental platform of the IPMSM drive control system is shown in Figure 10.

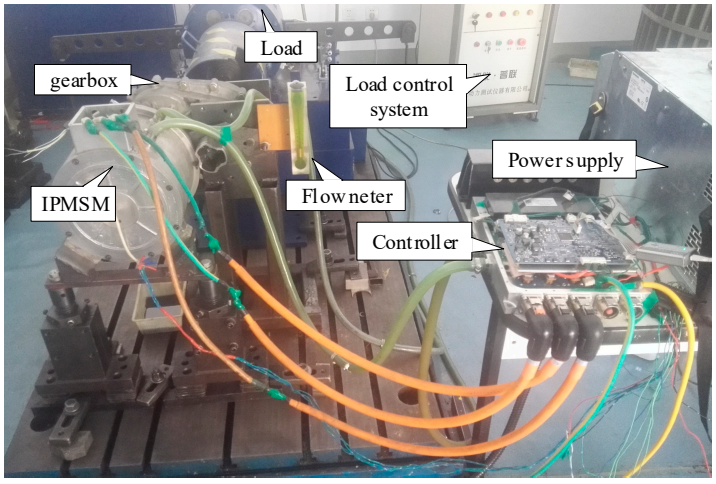

Figure 10. Experimental platform.

Setting the motor speed to 1250 r/min, the load torque was 9 N · m in 0–10 s. The experimental waveforms of the rotor position estimation of the conventional and the improved observer are shown in Figures 11 and 12.

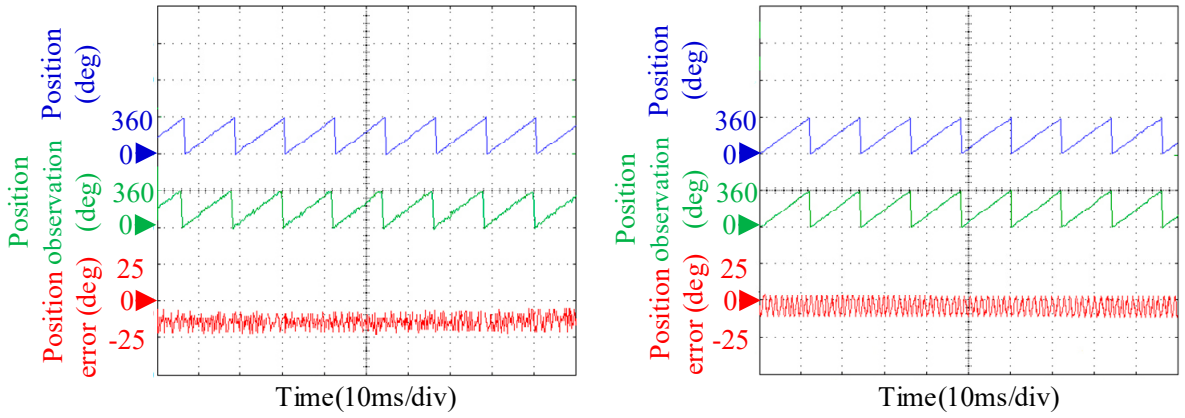

Figure 11. Experimental curves of the rotor position estimation.

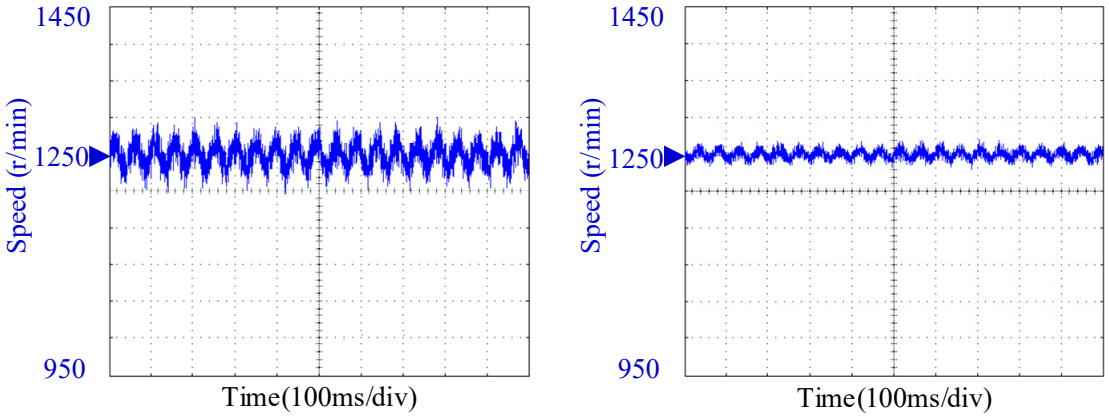

(**a**) CSMO (**b**) STA-SMO

Figure 12. Experimental curves of the speed estimation.

A significant position error exists between the actual value of the position and the observed value, through the CSMO. The average value of the position error is about 13.5°. The position error value of the STA-SMO is 5.1°; the signal has phase noise caused by switch chattering, and its peak value is 14°. Since the CSMO position signal is added by the low-pass filter, the phase lag of the observed value is obvious; the position error of the STA-SMO is smaller than that of the CSMO. The STA-SMO has the better suppression effect on chattering and reduces the phase deviation caused by the low-pass filter that was introduced. The STA-SMO is obviously better than CSMO, and it has a high accuracy and a small observation error for the rotor position estimation.

The speed fluctuation of the CSMO is ±50 r/min, while the speed fluctuation of the STA-SMO is only ±15 r/min. Compared with the CSMO, the STA-SMO has little effect on the speed fluctuation and has the better speed stability.

When the load torque was 9 N·m, the motor resistance was $R_s = 1.2\hat{R}_s$, the motor inductances were $L_d = 1.2\hat{L}_d$ and $L_q = 0.8\hat{L}_q$, the motor speed was 1250 r/min in 0–0.3 s, increased to 2500 r/min when t = 0.3 s, and decreased to 1250 r/min when t = 1.3 s. The experimental waveforms of the actual speed, the position signal observation value, and the position observation error of the STA-SMO and the STA-SMO with APEC are shown in Figures 13 and 14.

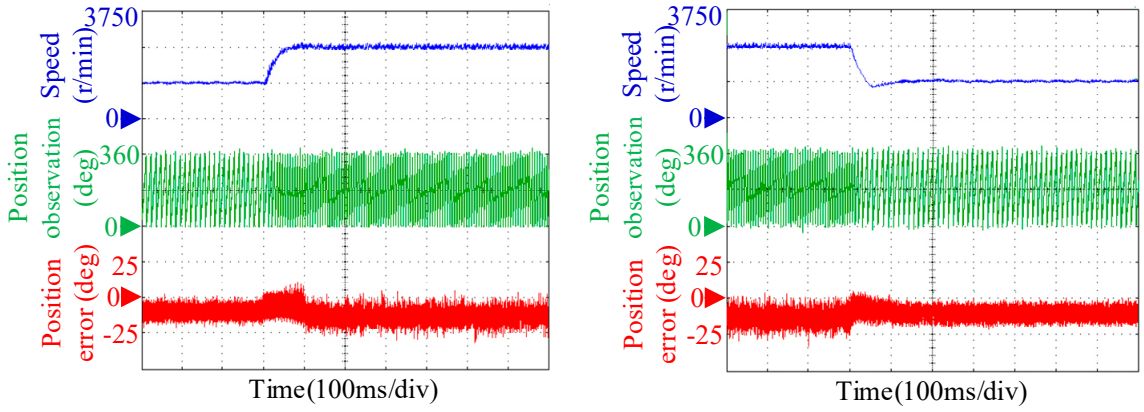

(**a**) Speed increased (**b**) Speed reduced

Figure 13. Experimental curves of speed response of STA-SMO.

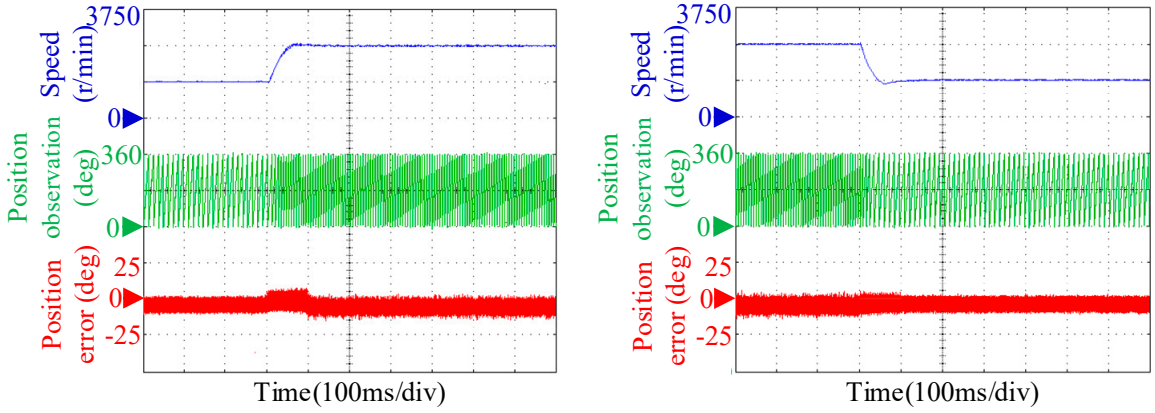

(**a**) Speed increased (**b**) Speed reduced

Figure 14. Experimental curves of speed response of STA-SMO with APEC.

When the position signal observation value chattering was increased, the noise was increased with the increase of motor power throughout the STA-SMO parameters mismatched with the motor's actual parameters. When the speed was 1250 r/min, the observation error was 10.2°. When the speed was 2500 r/min, the observation error was 16.6°. The position error and noise of the STA-SMO were larger in the dynamic adjustment process of the speed mutation, while the position error value of the STA-SMO with APEC was smaller, and the dynamic process was more stable.

The parameter deviation of the STA-SMO led to phase error in the estimation of the back EMF. After the step of the motor speed increased, the phase error was further increased because of the increase of motor load power. However, the STA-SMO with APEC effectively estimated the back EMF and subsequently reduced the observation error of the position signal, which adjusted the observer parameters in real time by estimating the motor parameters. The large fluctuation of the speed was caused by the parameter mismatch of the STA-SMO, while the STA-SMO with APEC can effectively improve the speed accuracy under the condition of parameter mismatch.

7. Results and Discussion

The phase lag of the CSMO is obvious and is caused by the low-pass filter, under the full load (9 N · m) and the 1250 r/min speed. The position error was reduced by 62.2%, and the speed fluctuation was reduced by 70% through the STA-SMO. The problem of poor observation accuracy of the CSMO was solved by the STA-SMO effectively. In [16–20], the switch function of the SMO was treated by the integral action of the high-order sliding mode approach law, but the high-order sliding mode approach law model is complex. By contrast, the parameters of the STA-SMO are fewer, the parameter

tuning is simple, and the debugging is relatively more convenient. Compared with the SPMSM [23], the deviation of the parameters, the current, the current change rate and the speed of the IPMSM have complex effects on the amplitude and the phase of the back EMF estimation. The APEC combined with Lyapunov's stability law to design the adaptive law of the resistance and inductance parameters to improve the robustness of the IPMSM parameter mismatches was proposed in this paper. The load torque was set to 9 N·m, the motor resistance was $R_s = 1.2\hat{R}_s$, the motor inductances were $L_d = 1.2\hat{L}_d$ and $L_q = 0.8\hat{L}_q$. When the speed was 1250 r/min, the observation error was reduced by 50% through the STA-SMO with the APEC. When the speed was 2500 r/min, the observation error was reduced by 64.5% through the STA-SMO with the APEC. The solution of the accuracy improvement of the back EMF observation under the dq-axis inductance parameter mismatch was not proposed by the methods in [26–29]. Meanwhile, the methods did not take into account the characteristics of the dq-axis inductance inequality of the IPMSM, which are limited to the SPMSM. The APEC not only effectively tracks the change of the resistance parameter and effectively suppresses the influence of the motor resistance parameter on the observation results, but it also tracks the actual value of the IPMSM dq-axis inductance. It effectively solves the influence of the back EMF estimation by inductance parameter mismatches and improves observation accuracy.

8. Conclusions

In this paper, a sliding mode observer control method based on the super twisting algorithm with adaptive parameter estimation control was proposed for the sensorless control of IPMSM. To solve the chattering and filters, the high-order approach law of the super twisting algorithm, which has integral effect on the switching function, effectively improved the convergence speed of the system and enhanced the observation accuracy of the rotor position and speed. Because the change of motor parameters affects the amplitude and phase of the back EMF and further affects the stability of the system, the regulation of the stator resistances and of the inductances, which was derived from Lyapunov's stability equation, was used to update the observer parameters in real time; it effectively suppressed the influence of the change of motor parameters on the observer observation results and has strong robustness.

In the future, the method that updates the motor parameters in real time and reduces the observation error will be extended to low speed range to realize a wide speed range operation. However, the back EMF of the motor is too small to be estimated during the zero speed and ultra-low speed. We plan to verify a current closed-loop start strategy that can solve the working condition of the motor starting or in ultra-low speed operation. In this strategy, the speed loop feedback value is replaced by the rotor position angle generator, and the current closed loop reference value and rotor position angle are designed by the motor starting acceleration.

Author Contributions: Conceptualization, Y.L.; Methodology, Y.L.; Software, Y.L.; Validation, Y.L.; Formal Analysis, K.T.; Investigation, Y.L.; Resources, J.F.; Data Curation, Y.L.; Writing—Original Draft Preparation, Y.L.; Writing—Review & Editing, B.H. and W.H.; Visualization, Y.L.; Supervision, J.F.; Project Administration, Y.L.; Funding Acquisition, J.F. All authors have read and agreed to the published version of the manuscript.

Funding: This research was supported by the Application Technology Researchand Development of Harbin, under Grant 2017RAXXJ075.

Conflicts of Interest: The authors declare no conflict of interest.

References

1. Lyu, M.; Wu, G.; Luo, D.; Rong, F.; Huang, S. Robust Nonlinear Predictive Current Control Techniques for PMSM. *Energies* **2019**, *12*, 443. [CrossRef]
2. Andreescu, G.D.; Pitic, C.; Blaabjerg, F.; Boldea, I. Combined Flux Observer with Signal Injection Enhancement for Wide Speed Range Sensorless Direct Torque Control of IPMSM Drives. *IEEE Trans. Energy Convers.* **2008**, *23*, 393–402. [CrossRef]

3. Yin, Z.; Li, G.; Zhang, Y.; Liu, J. Symmetric-Strong-Tracking-Extended-Kalman-Filter-Based Sensorless Control of Induction Motor Drives for Modeling Error Reduction. *IEEE Trans. Ind. Inform.* **2019**, *15*, 650–662. [CrossRef]
4. Bhuyan, A.; Tudu, B.; Bandopadhyay, R.; Ghosh, A.; Kumar, S. Extended Kalman Filtering for Estimation of Parasitic Artifacts in Three Electrode Electrochemical Sensors. *IEEE Sens. Lett.* **2019**, *3*, 1–4. [CrossRef]
5. Duan, P.H.; Duan, Z.H.; Lyu, Y.Z.; Chen, G. Distributed Finite-Horizon Extended Kalman Filtering for Uncertain Nonlinear Systems. *IEEE Trans. Cybern.* **2019**, 2111–2115. [CrossRef]
6. Gao, Q.; Asher, G.; Sumner, M. Sensorless Position and Speed Control of Induction Motors Using High-Frequency Injection and Without Offline Precommissioning. *IEEE Trans. Ind. Electron.* **2007**, *54*, 2474–2481. [CrossRef]
7. Barut, M.; Bogosyan, S.; Gokasan, M. Speed-Sensorless Estimation for Induction Motors Using Extended Kalman Filters. *IEEE Trans. Ind. Electron.* **2007**, *54*, 272–280. [CrossRef]
8. Holtz, J.; Quan, J. Sensorless vector control of induction motors at very low speed using a nonlinear inverter model and parameter identification. *IEEE Trans. Ind. Appl.* **2002**, *38*, 1087–1088. [CrossRef]
9. Marko, H.; Jorma, L. Stabilization of regenerating-mode operation in sensorless induction motor drives by full-order flux observer design. *IEEE Trans. Ind. Electr.* **2004**, *51*, 1318–1319.
10. Alessandri, A. Sliding-mode estimators for a class of non-linear systems affected by bounded disturbances. *Int. J. Control* **2003**, *76*, 226–236. [CrossRef]
11. Xiong, Y.; Saif, M. Sliding mode observer for nonlinear uncertain systems. *IEEE Trans. Autom. Control* **2001**, *46*, 2012–2017. [CrossRef]
12. Zhang, X.; Li, Z. Sliding-Mode Observer-Based Mechanical Parameter Estimation for Permanent Magnet Synchronous Motor. *IEEE Trans. Power Electron.* **2016**, *31*, 5732–5745. [CrossRef]
13. Khayati, K. Multivariable Adaptive Sliding-Mode Observer-Based Control for Mechanical Systems Mode de glissement adaptatif etmulti-variable pour un contrôle basé sur un observateur pour les systèmes mécaniques. *Can. J. Electr. Comput. Eng.* **2015**, *38*, 253–254. [CrossRef]
14. Sun, J.; Cao, G.-Z.; Huang, S.-D.; Peng, Y.; He, J.; Qian, Q.-Q. Sliding-Mode-Observer-Based Position Estimation for Sensorless Control of the Planar Switched Reluctance Motor. *IEEE Access* **2019**, *7*, 61034–61045. [CrossRef]
15. Lin, C.; Sun, S.; Walker, P.; Zhang, N. Accelerated Adaptive Second Order Super-Twisting Sliding Mode Observer. *IEEE Access* **2019**, *7*, 25232–25238. [CrossRef]
16. Liu, C.; Cai, G.; Gao, J.; Yang, D. Design of Nonlinear Robust Damping Controller for Power Oscillations Suppressing Based on Backstepping-Fractional Order Sliding Mode. *Energies* **2017**, *10*, 676. [CrossRef]
17. Gao, P.; Zhang, G.; Ouyang, H.; Mei, L. An Adaptive Super Twisting Nonlinear Fractional Order PID Sliding Mode Control of Permanent Magnet Synchronous Motor Speed Regulation System Based on Extended State Observer. *IEEE Access* **2020**, *8*, 53498–53510. [CrossRef]
18. Yang, Z.B.; Zhang, D.; Sun, X.D.; Ye, X. Adaptive Exponential Sliding Mode Control for a Bearingless Induction Motor Based on a Disturbance Observer. *IEEE Access* **2018**, *6*, 35425–35426. [CrossRef]
19. Sun, X.; Chen, L.; Yang, Z. Overview of Bearingless Permanent-Magnet Synchronous Motors. *IEEE Trans. Ind. Electron.* **2013**, *60*, 5528–5538. [CrossRef]
20. Yang, J.; Li, S.; Yu, X. Sliding-mode control for systems with mismatched uncertainties via a disturbance observer. *IEEE Trans. Ind. Electr.* **2013**, *60*, 160–161. [CrossRef]
21. Wang, G.; Zhou, C.; Yu, Y.; Liu, X. Adaptive Sliding Mode Trajectory Tracking Control for WMR Considering Skidding and Slipping via Extended State Observer. *Energies* **2019**, *12*, 3305. [CrossRef]
22. Liang, D.L.; Li, J.; Qu, R.H. Adaptive Second Order Sliding Mode Observer for PMSM Sensorless Control Considering VSI Nonlinearity. *IEEE Trans. Power Electr.* **2018**, *33*, 8994–9000. [CrossRef]
23. Li, Z.; Zhou, S.; Xiao, Y.; Wang, L. Sensorless Vector Control of Permanent Magnet Synchronous Linear Motor Based on Self-Adaptive Super-Twisting Sliding Mode Controller. *IEEE Access* **2019**, *7*, 44998–45000. [CrossRef]
24. Wang, H.; Ge, X.; Liu, Y.-C. Second-Order Sliding-Mode MRAS Observer-Based Sensorless Vector Control of Linear Induction Motor Drives for Medium-Low Speed Maglev Applications. *IEEE Trans. Ind. Electron.* **2018**, *65*, 9938–9952. [CrossRef]
25. Davila, J.; Fridman, L.; Levant, A. Second-order sliding-mode observer for mechanical systems. *IEEE Trans. Autom. Control* **2005**, *50*, 1785–1789. [CrossRef]

26. Lu, W.; Zhang, Z.; Wang, D.; Lu, K.; Wu, D.; Ji, K.; Guo, L. A New Load Torque Identification Sliding Mode Observer for Permanent Magnet Synchronous Machine Drive System. *IEEE Trans. Power Electron.* **2019**, *34*, 7852–7862. [CrossRef]
27. Liang, D.L.; Li, J.; Qu, R.H. Sensorless Control of Permanent Magnet Synchronous Machine Based on Second-Order Sliding-Mode Observer with Online Resistance Estimation. *IEEE Trans. Ind. Appl.* **2017**, *53*, 3672–3673. [CrossRef]
28. Zhao, L.; Huang, J.; Liu, H.; Li, B.; Kong, W. Second-Order Sliding-Mode Observer with Online Parameter Identification for Sensorless Induction Motor Drives. *IEEE Trans. Ind. Electron.* **2014**, *61*, 5280–5289. [CrossRef]
29. Qiao, Z.; Shi, T.; Wang, Y.; Yan, Y.; Shi, T.; He, X. New Sliding-Mode Observer for Position Sensorless Control of Permanent-Magnet Synchronous Motor. *IEEE Trans. Ind. Electron.* **2013**, *60*, 710–719. [CrossRef]
30. Zhang, W.; Wang, W.; Liu, H.; Xu, D. A Disturbance Rejection Control Strategy for Droop-Controlled Inverter Based on Super-Twisting Algorithm. *IEEE Access* **2019**, *7*, 27037–27046. [CrossRef]
31. Lin, C.; Sun, S.X.; Yi, J.; Walker, P.; Zhang, N. Accelerated adaptive super twisting sliding mode observer-based drive shaft torque estimation for electric vehicle with automated manual transmission. *IET Intell. Transp. Syst.* **2019**, *13*, 160–162. [CrossRef]